JOURNAL OF GUIDANCE, CONTROL, AND DYNAMICS
Vol. 29, No. 2, March–April 2006

Tensor-Product Model-Based Control of Two-Dimensional Aeroelastic System

Péter Baranyi*
Computer and Automation Research Institute of the Hungarian Academy of Sciences, H-1111 Budapest, Hungary

Use of a recently introduced numerical robust-control design method to stabilize aeroelastic systems according to different control specifications is studied. This numerical design is based on the tensor-product model transformation and the parallel-distributed-compensation design framework. An alternative description of aeroelastic models is also proposed as a gateway to various recent linear-matrix-inequality-based control theories. This study is conducted through an example that focuses attention on the state-variable-feedback controller design to the prototypical aeroelastic wing section with structural nonlinearity. This type of model has been traditionally used for the theoretical as well as experimental analysis of two-dimensional aeroelastic behavior and exhibits limit-cycle oscillation without control effort. Numerical simulations to provide empirical validation of the resulting controllers are presented. Comparison to former alternative control solutions is also presented.

Nomenclature†

a	=	nondimensional distance from the midchord to the elastic axis
b	=	semichord of the wing
c_h	=	plunge structural-damping coefficients
c_{l_α}	=	lift coefficients per angle of attack
c_{l_β}	=	lift coefficients per control surface deflection
c_{m_α}	=	moment coefficients per angle of attack
c_{m_β}	=	moment coefficients per control surface deflection
c_α	=	pitch structural-damping coefficient
h	=	plunging displacement
I_α	=	mass moment of inertia
k_h	=	plunge structural-spring constant
$k_\alpha(\alpha)$	=	nonlinear stiffness contribution
L	=	aerodynamic force
M	=	aerodynamic moment
m	=	mass of the wing
U	=	free stream velocity
x_α	=	nondimensional distance between elastic axis and the center of mass
α	=	pitching displacement
β	=	control surface deflection
ρ	=	air density

Introduction

In the past few years various studies of aeroelastic systems have emerged. One can find a whole series of detailed studies of this topic in the *Journal of Guidance, Control, and Dynamics*.

Regarding the properties of aeroelastic systems, one can find the study of free-play nonlinearity by Price et al. in Refs. 2 and 3 and by Lee and LeBlanc in Ref. 4, and a complete study of a class of nonlinearities in Refs. 3 and 5. O'Neil and Strganac[6] examined the continuous structural nonlinearity of aeroelastic systems. Recent analysis is given in Ref. 7. These papers conclude that an aeroelastic system may exhibit a variety of nonlinear phenomena such as limit-cycle oscillation, flutter, and even chaotic vibrations.

Control strategies have also been derived for aeroelastic systems. Block and Strganac[8] show that in the case of large-amplitude limit-cycle oscillation behavior the linear-control methodologies do not stabilize aeroelastic systems consistently. At the NASA Langley Research Center, a benchmark active-control technique (BACT) wind-tunnel model has been designed and control algorithms for flutter suspension have been developed by Waszak,[9] Mukhopadhyay,[10] and Kelkar and Joshi.[11] For an aeroelastic apparatus, tests have been performed in a wind tunnel to examine the effect of nonlinear structural stiffness, and control systems have been designed using linear-control theory, feedback-linearization technique, and adaptive-control strategies.[12–14]

One can find studies focusing attention on the two-dimensional prototypical aeroelastic wing section. Block and Strganac[8] and Ko et al.[15] proposed nonlinear-feedback-control methodologies for a class of nonlinear structural effects of the prototypical aeroelastic wing section.[16] In this regard Ko et al.[13] develop a controller via partial-feedback linearization. It has been shown that global stabilization can be achieved by applying an additional control surface. For instance, see Ref. 17. Adaptive-feedback linearization and the global-feedback-linearization technique were introduced for two control actuators in Refs. 12 and 13, and the Riccati-equation-based method was used in Ref. 18. Neural-network-based design was also discussed in Ref. 19.

The contribution of this paper is to continue these control studies on the prototypical aeroelastic wing section. The aim of the study is to design flutter control by state-variable feedback capable of satisfying various control specifications.

We apply the recently introduced tensor-product (TP) model transformation[20,21] to transform the parameter-varying state-space model of the prototypical aeroelastic wing into the tensor-product model whereupon the parallel-distributed-compensation (PDC) design framework can be executed immediately.[22] The PDC framework is based on the feasibility test of linear matrix inequalities (LMI) constructed according to various stability and other control specifications. We apply MATLAB® LMI Control Toolbox for the feasibility test of the constructed LMIs.[23] The main advantage of this alternative design is that it guarantees asymptotic stability via single trailing-edge control surface, and, beyond stability, is readily capable of involving a variety of different design specifications in contrast with former control solutions. In this regard we focus attention on the speed of response (decay-rate optimization) and constraints on the control value.

An additional contribution of this paper is to show that the prototypical aeroelastic wing section can be described exactly by the time-varying convex combination of six linear-time-invariant (LTI)

Received 23 March 2004; revision received 15 October 2004; accepted for publication 5 August 2005.

*Professor, Kende u. 13-17; also Integrated Intelligent Systems Japanese–Hungarian Laboratory, H-1111 Budapest, Műegyetem rakpart 3., Hungary; baranyi@tmit.bme.hu.

†Papers dealing with the TP model transformation apply tensor notation. In this regard we refer to Ref. 1.

models. This alternative model representation is the result of the TP model transformation and has not been investigated in previous studies of the aeroelastic models. The advantage of this alternative representation is that it may open a gate to various recent LMI-based design techniques. This advantage is exploited in the present case study.

Although this paper focuses attention on the analytically given two-dimensional prototypical aeroelastic-wing-section model, the applied design methodology can be applied to a variety (even more complex forms) of aeroelastic models. The reason is that all the steps of the discussed design method are executable numerically in a reasonable time and it is irrelevant whether the given explicit model is a physical model or just an outcome of a black-box identification.

Equations of Motion

To be comparable with previous studies about the prototypical aeroelastic wing section, we adopt the same simplified equations of motion as investigated in various works, for example, Refs. 12, 14, 17, 24, and 25. We consider the problem of flutter suppression for the prototypical aeroelastic wing section as shown in Fig. 1. The flat plate airfoil is constrained to have two degrees of freedom, the plunge h and pitch α. The equations of motion can be written as

$$\begin{pmatrix} m & mx_\alpha b \\ mx_\alpha b & I_\alpha \end{pmatrix}\begin{pmatrix} \ddot{h} \\ \ddot{\alpha} \end{pmatrix} + \begin{pmatrix} c_h & 0 \\ 0 & c_\alpha \end{pmatrix}\begin{pmatrix} \dot{h} \\ \dot{\alpha} \end{pmatrix} + \begin{pmatrix} k_h & 0 \\ 0 & k_\alpha(\alpha) \end{pmatrix}\begin{pmatrix} h \\ \alpha \end{pmatrix} = \begin{pmatrix} -L \\ M \end{pmatrix} \tag{1}$$

We obtain $k_\alpha(\alpha)$ by curve-fitting on the measured displacement-moment data for nonlinear spring[5]:

$$k_\alpha(\alpha) = 2.82\,(1 - 22.1\alpha + 1315.5\alpha^2 + 8580\alpha^3 + 17{,}289.7\alpha^4)$$

We assume the quasi-steady aerodynamic force and moment, as in the previous control design approaches:

$$L = \rho U^2 b c_{l_\alpha}\left[\alpha + \dot{h}/U + \left(\tfrac{1}{2} - a\right)b(\dot{\alpha}/U)\right] + \rho U^2 b c_{l_\beta}\beta$$

$$M = \rho U^2 b^2 c_{m_\alpha}\left[\alpha + \dot{h}/U + \left(\tfrac{1}{2} - a\right)b(\dot{\alpha}/U)\right] + \rho U^2 b c_{m_\beta}\beta \tag{2}$$

L and M are accurate for the class of low velocity. Wind-tunnel experiments are carried out in Ref. 7. The system parameters used are given in the Appendix. These data are obtained from experimental models described in full detail in Refs. 6 and 12. With the flow velocity $u = 15$ m/s and the initial values of $\alpha = 0.1$ rad and $h = 0.01$ m, the resulting time response of the nonlinear system is depicted in Fig. 2. We remark that the response will achieve limit-cycle oscillation as claimed in Refs. 5, 6, and 12. O'Neil and Strganac[6] and O'Neil et al.[16] have shown the relations between limit-cycle oscillation, magnitudes, and initial conditions or flow velocities.

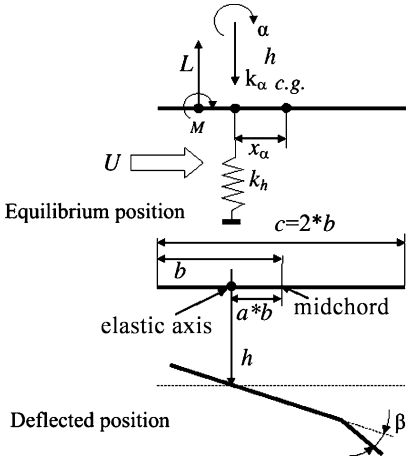

Fig. 1 Two-dimensional flat plate airfoil small deflection, force notation, and schematic diagram.

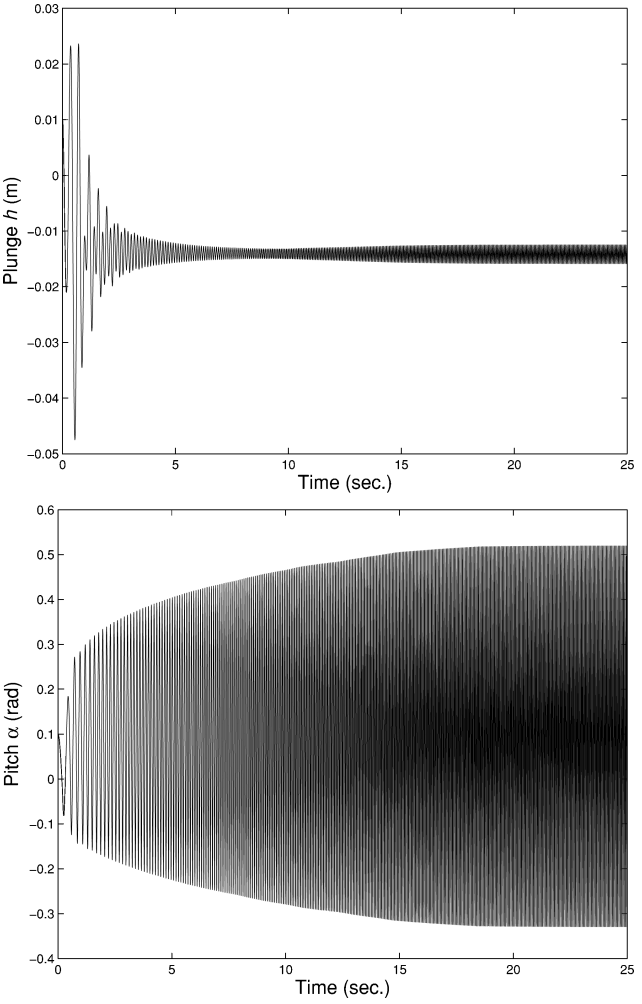

Fig. 2 Open-loop response for plunge (h) and pitch (α) motion is shown for $U = 20$ m/s and $a = -0.4$.

By combining equations (1) and (2), one obtains

$$\begin{pmatrix} m & mx_\alpha b \\ mx_\alpha b & I_\alpha \end{pmatrix}\begin{pmatrix} \ddot{h} \\ \ddot{\alpha} \end{pmatrix} + \begin{pmatrix} c_h + \rho U b c_{l_\alpha} & \rho U b^2 c_{l_\alpha}\left(\frac{1}{2} - a\right) \\ \rho U b^2 c_{m_\alpha} & c_\alpha - \rho U b^3 c_{m_\alpha}\left(\frac{1}{2} - a\right) \end{pmatrix}\begin{pmatrix} \dot{h} \\ \dot{\alpha} \end{pmatrix} + \begin{pmatrix} k_h & \rho U^2 b c_{l_\alpha} \\ 0 & -\rho U^2 b^2 c_{m_\alpha} + k_\alpha(\alpha) \end{pmatrix}\begin{pmatrix} h \\ \alpha \end{pmatrix} = \begin{pmatrix} \rho b c_{l_\beta} \\ \rho b^2 c_{m_\beta} \end{pmatrix} U^2\beta \tag{3}$$

For control design, Eq. (3) was converted into state-space formulation. Let

$$\boldsymbol{x}(t) = \begin{pmatrix} x_1(t) \\ x_2(t) \\ x_3(t) \\ x_4(t) \end{pmatrix} = \begin{pmatrix} h \\ \alpha \\ \dot{h} \\ \dot{\alpha} \end{pmatrix}$$

and $\boldsymbol{u}(t) = \beta$. Then we have

$$\dot{\boldsymbol{x}}(t) = \boldsymbol{A}[\boldsymbol{p}(t)]\boldsymbol{x}(t) + \boldsymbol{B}[\boldsymbol{p}(t)]\boldsymbol{u}(t) = \boldsymbol{S}[\boldsymbol{p}(t)]\begin{pmatrix} \boldsymbol{x}(t) \\ \boldsymbol{u}(t) \end{pmatrix} \tag{4}$$

where

$$\boldsymbol{A}[\boldsymbol{p}(t)] = \begin{pmatrix} 0 & 0 & 1 & 0 \\ 0 & 0 & 0 & 1 \\ -k_1 & -\left(k_2 U^2 + p(x_2(t))\right) & -c_1(U) & -c_2(U) \\ -k_3 & -\left(k_4 U^2 + q(x_2(t))\right) & -c_3(U) & -c_4(U) \end{pmatrix}$$

$$\boldsymbol{B}(\boldsymbol{p}(t)) = \begin{pmatrix} 0 \\ 0 \\ g_3 U^2 \\ g_4 U^2 \end{pmatrix}$$

and $\boldsymbol{p}(t) \in \mathbb{R}^{N=2}$ contains values $x_2(t) = \alpha$ and U. The new variables are given in the Appendix. Note that the equations of motion are also dependent upon the elastic axis location a.

Basic Concepts

Linear Parameter-Varying State-Space Model

Consider parameter-varying state-space model:

$$\dot{\boldsymbol{x}}(t) = \boldsymbol{A}[\boldsymbol{p}(t)]\boldsymbol{x}(t) + \boldsymbol{B}[\boldsymbol{p}(t)]\boldsymbol{u}(t)$$

$$\boldsymbol{y}(t) = \boldsymbol{C}[\boldsymbol{p}(t)]\boldsymbol{x}(t) + \boldsymbol{D}[\boldsymbol{p}(t)]\boldsymbol{u}(t) \tag{5}$$

with input $\boldsymbol{u}(t)$, output $\boldsymbol{y}(t)$, and state vector $\boldsymbol{x}(t)$. The system matrix

$$\boldsymbol{S}[\boldsymbol{p}(t)] = \begin{pmatrix} \boldsymbol{A}[\boldsymbol{p}(t)] & \boldsymbol{B}[\boldsymbol{p}(t)] \\ \boldsymbol{C}[\boldsymbol{p}(t)] & \boldsymbol{D}[\boldsymbol{p}(t)] \end{pmatrix} \tag{6}$$

is a parameter-varying object, where $\boldsymbol{p}(t) \in \Omega$ is time varying N-dimensional parameter vector, where $\Omega = [a_1, b_1] \times [a_2, b_2] \times \cdots \times [a_N, b_N] \subset \mathbb{R}^N$ is a closed hypercube. Parameter $\boldsymbol{p}(t)$ can also include some elements of $\boldsymbol{x}(t)$. Assume that the size of the system matrix $\boldsymbol{S}(\boldsymbol{p}(t))$ is O times I.

Tensor-Matrix Product

This subsection defines some basic tensor operations used later in this paper.

Definition 1 (n-mode matrix of tensor $\mathcal{A}$): Assume an Nth-order tensor $\mathcal{A} \in \mathbb{R}^{I_1 \times I_2 \times \cdots \times I_N}$. The n-mode matrix $\boldsymbol{A}_{(n)} \in \mathbb{R}^{I_n \times J}$, $J = \prod_k I_k$ contains all the vectors in the nth dimension of tensor $\mathcal{A}$, where $k = 1, \ldots, N$ and $k \neq n$. The ordering of the vectors is arbitrary in $\boldsymbol{A}_{(n)}$. This ordering shall, however, be consistently used later. $(\boldsymbol{A}_{(n)})_j$ is called an jth n-mode vector.

Note that any matrix of which the columns are given by n-mode vectors $(\boldsymbol{A}_{(n)})_j$ can readily be restored to become tensor $\mathcal{A}$. The restoration can be executed even in case when some rows of $\boldsymbol{A}_{(n)}$ are discarded because the value of I_n has no role in the ordering of $(\boldsymbol{A}_{(n)})_j$ (Ref. 1).

Definition 2 (n-mode matrix-tensor product): The n-mode product of tensor $\mathcal{A} \in \mathbb{R}^{I_1 \times I_2 \times \cdots \times I_N}$ and a matrix $\boldsymbol{U} \in \mathbb{R}^{J \times I_n}$, as denoted by $\mathcal{A} \times_n \boldsymbol{U}$, is an $(I_1 \times I_2 \times \cdots \times I_{n-1} \times J \times I_{n+1} \times \cdots \times I_N)$ tensor of which the entries are given by $A \times_n \boldsymbol{U} = B$, where $\boldsymbol{B}_{(n)} = \boldsymbol{U} \cdot \boldsymbol{A}_{(n)}$. Let $\mathcal{A} \times_1 \boldsymbol{U}_1 \times_2 \boldsymbol{U}_2 \times \cdots \times_N \boldsymbol{U}_N$ be denoted as $\mathcal{A} \otimes_{n=1}^{N} \boldsymbol{U}_n$ for brevity.

Definition 3 (n-mode rank of tensor $\mathcal{A}$): The n-mode rank of $\mathcal{A}$, denoted by $R_n = \text{rank}_n(\mathcal{A})$, is the dimension of the vector space spanned by the n-mode matrices as $\text{rank}_n(\mathcal{A}) = \text{rank}(\boldsymbol{A}_{(n)})$.

Convex State-Space Tensor-Product Model

Equation (6) can be approximated for any parameter $\boldsymbol{p}(t)$ as a convex combination of the R LTI system matrices $\boldsymbol{S}_r$, $r = 1 \ldots R$. Matrices $\boldsymbol{S}_r$ are also termed as vertex-system matrices. Therefore, one can define basis functions $w_r(\boldsymbol{p}(t)) \in [0, 1] \subset \mathbb{R}$ such that matrix $\boldsymbol{S}(\boldsymbol{p}(t))$ belongs to the convex hull of $\boldsymbol{S}_r$ as $\boldsymbol{S}(\boldsymbol{p}(t)) = co\{\boldsymbol{S}_1, \boldsymbol{S}_2, \boldsymbol{S}_R\}_{w(p(t))}$, where vector $\boldsymbol{w}[\boldsymbol{p}(t)]$ contains the basis functions $w_r(\boldsymbol{p}(t))$ of the convex combination

$$\boldsymbol{S}[\boldsymbol{p}(t)] \approx \sum_{r=1}^{R} w_r[\boldsymbol{p}(t)]\boldsymbol{S}_r$$

The control-design methodology, applied in this paper, uses one-variable basis functions. This means that each variable has its own basis-function system. Or, one can say that the multivariable basis $w_r(\boldsymbol{p}(t))$ is decomposed to the product of univariate basis functions. Thus, the explicit form of the convex combination in terms of tensor product becomes

$$\boldsymbol{S}[\boldsymbol{p}(t)] \approx \sum_{i_1=1}^{I_1} \sum_{i_2=1}^{I_2} \cdots \sum_{i_N=1}^{I_N} \prod_{n=1}^{N} w_{n,i_n}[p_n(t)]\boldsymbol{S}_{i_1,i_2,\ldots,i_N}$$

where $w_r[\boldsymbol{p}(t)] = \prod_{n=1}^{N} w_{n,i_n}(p_n(t))$, $\boldsymbol{S}_r = \boldsymbol{S}_{i_1,i_2,\ldots,i_N}$ and $p_n(t)$ is the nth element of vector $\boldsymbol{p}(t)$.

Therefore

$$\begin{pmatrix} s\boldsymbol{x}(t) \\ \boldsymbol{y}(t) \end{pmatrix} \approx \left(\sum_{i_1=1}^{I_1} \sum_{i_2=1}^{I_2} \cdots \sum_{i_N=1}^{I_N} \prod_{n=1}^{N} w_{n,i_n}[p_n(t)]\boldsymbol{S}_{i_1,i_2,\ldots,i_N} \right) \begin{pmatrix} \boldsymbol{x}(t) \\ \boldsymbol{u}(t) \end{pmatrix} \tag{7}$$

Model (7) is termed as TP model in this paper. Function $w_{n,j}(p_n(t)) \in [0, 1]$ is the jth univariate basis function defined on the nth dimension of Ω. $I_n (n = 1, \ldots, N)$ is the number of univariate basis functions used in the nth dimension of the parameter vector $\boldsymbol{p}(t)$. The multiple index $(i_1, i_2, \ldots, i_N)$ refers to the LTI system corresponding to the i_nth basis function in the nth dimension. Hence, the number of LTI vertex systems $\boldsymbol{S}_{i_1,i_2,\ldots,i_N}$ is obviously $R = \prod_n I_n$. One can rewrite relation (7) in the concise TP form as (see Appendix)

$$\begin{pmatrix} s\boldsymbol{x}(t) \\ \boldsymbol{y}(t) \end{pmatrix} \approx \mathcal{S} \underset{n=1}{\overset{N}{\otimes}} \boldsymbol{w}_n[p_n(t)] \begin{pmatrix} \boldsymbol{x}(t) \\ \boldsymbol{u}(t) \end{pmatrix}$$

$$\text{that is,} \qquad \boldsymbol{S}[\boldsymbol{p}(t)] \underset{\varepsilon}{\approx} \mathcal{S} \underset{n=1}{\overset{N}{\otimes}} \boldsymbol{w}_n[p_n(t)] \tag{8}$$

Here, ε symbolizes the approximation error, row vector $\boldsymbol{w}_n(p_n) \in \mathbb{R}^{I_n}$ contains the basis functions $w_{n,i_n}(p_n)$, the $N+2$–dimensional coefficient tensor $S \in \mathbb{R}^{I_1 \times I_2 \times \cdots \times I_N \times O \times I}$ is constructed from the LTI vertex system matrices $\boldsymbol{S}_{i_1,i_2,\ldots,i_N} \in \mathbb{R}^{O \times I}$. The first N dimensions of S are assigned to the dimensions of Ω.

For instance, assume a state-space model

$$\dot{\boldsymbol{x}}(t) = \boldsymbol{A}[\boldsymbol{p}(t)]\boldsymbol{x}(t) + \boldsymbol{B}[\boldsymbol{p}(t)]\boldsymbol{u}(t)$$

where the parameter vector is two-dimensional $\boldsymbol{p}(t) = (x_1(t) \;\; x_2(t))$, where $x_1(t)$ and $x_2(t)$ are the elements of state vector $\boldsymbol{x}(t)$. Then the state-space TP model form is

$$\dot{\boldsymbol{x}}(t) \approx \sum_{i=1}^{I} \sum_{j=1}^{J} w_{1,i}[x_1(t)]w_{2,j}[x_2(t)][\boldsymbol{A}_{i,j}\boldsymbol{x}(t) + \boldsymbol{B}_{i,j}\boldsymbol{u}(t)] \tag{9}$$

In terms of tensors, Eq. (9) takes the form

$$\dot{\boldsymbol{x}}(t) \approx \mathcal{A} \times_1 \boldsymbol{w}_1[x_1(t)] \times_2 \boldsymbol{w}_2[x_2(t)] \times_4 \boldsymbol{x}^T(t) + \mathcal{B} \times_1 \boldsymbol{w}_1[x_1(t)] \times_2 \boldsymbol{w}_2[x_2(t)] \times_4 \boldsymbol{u}^T(t)$$

Then, using the tensor-product notation, one can write

$$\dot{\boldsymbol{x}}(t) \approx \mathcal{S} \times_1 \boldsymbol{w}_1[x_1(t)] \times_2 \boldsymbol{w}_2[x_2(t)] \times_4 [\boldsymbol{x}^T(t) \quad \boldsymbol{u}^T(t)]$$

$$= \left\{ \mathcal{S} \underset{n=1}{\overset{2}{\otimes}} \boldsymbol{w}_n[x_n(t)] \right\} \begin{pmatrix} \boldsymbol{x}(t) \\ \boldsymbol{u}(t) \end{pmatrix} \tag{10}$$

For additional simple two-dimensional examples, see Ref. 21.

The convex combination of the LTI vertex systems is ensured by the following conditions.

Definition 4: The TP model (8) is convex if

$$\forall n, i,\ p_n(t) : w_{n,i}[p_n(t)] \in [0,\ 1] \tag{11}$$

$$\forall n,\ p_n(t) : \sum_{i=1}^{I_n} w_{n,i}[p_n(t)] = 1 \tag{12}$$

From an engineering point of view, this simply means that $\boldsymbol{S}(\boldsymbol{p}(t))$ varies within the convex hull of the LTI vertex systems $\boldsymbol{S}_{i_1,i_2,\ldots,i_N}$ for any $\boldsymbol{p}(t) \in \Omega$.

Remark 1: $\boldsymbol{S}(\boldsymbol{p}(t))$ has finite-element TP model representation in many cases [$\varepsilon = 0$ in relation (8)]. However, exact finite-element TP model representation does not exist in general [$\varepsilon > 0$ in relation (8)]; see Ref. 26. In this case $\varepsilon \mapsto 0$, when the number of LTI systems involved in the TP model goes to ∞. In the present control design, we will show that the dynamic model of the aeroelastic system can be exactly represented by a finite TP model.

We define here a further characteristic of the convex TP model.

Definition 5: The LTI vertex systems form a tight convex hull if their corresponding basis functions have the following feature:

$$\forall n, i_n; \max_{p_n(t)} \left(w_{n,i_n}[p_n(t)]\right) \underset{\delta_{n,i_n}}{\approx} 1 \tag{13}$$

where $\forall \delta_{n,i_n}$ as small as possible. For instance, the basis functions are determined subject to

$$\text{minimize } \left(\|\boldsymbol{\delta}\|_{L_2}\right)$$

where vector $\boldsymbol{\delta}$ consists of all $\boldsymbol{\delta}_{n,i_n}$.

Transformation of the Aeroelastic Model to TP-Model Form

First, we give a brief introduction to the TP model transformation based on Refs. 20 and 21.

TP-Model Transformation

The goal of the TP-model transformation is to transform a given state-space model [Eq. (5)] into convex TP model, where the LTI systems form a tight convex hull. Namely, the TP model transformation results in relation (8) with conditions (11) and (12), and searches the LTI systems as a points of a tight convex hull of $\boldsymbol{S}[\boldsymbol{p}(t)]$; see relation (13).

The TP-model transformation is a numerical method and has three key steps. The first step is the discretization of the given $\boldsymbol{S}(\boldsymbol{p}(t))$ via the sampling of $\boldsymbol{S}(\boldsymbol{p}(t))$ over a huge number of points $\boldsymbol{p} \in \Omega$. The sampling points are defined by a dense hyperrectangular grid. To lose minimal information during the discretization, we apply as dense a grid as possible. The second step extracts the LTI vertex systems from the sampled systems. This step is specialized to find the minimal number of LTI vertex systems as the vertex points of the tight convex hull of the sampled systems. The third step constructs the TP model based on the LTI vertex systems obtained in the second step. It defines the continuous basis functions to the LTI vertex systems.

Method 1: TP model transformation.

Step 1. Discretization. Define the transformation space Ω as $\boldsymbol{p}(t) \in \Omega : [a_1, b_1] \times [a_2, b_2] \times \cdots \times [a_N, b_N]$. Define a hyperrectangular grid by equidistantly located gridlines: $g_{n,m_n} = a_n + [(b_n - a_n)/(M_n - 1)](m_n - 1)$, $m_n = 1 \ldots M_n$. The numbers of the gridlines in the dimensions are M_n. Sample the given function $\boldsymbol{S}(\boldsymbol{p}(t))$ over the gridpoints:

$$\boldsymbol{S}^s_{m_1,m_2,\ldots,m_N} = \boldsymbol{S}(\boldsymbol{p}_{m_1,m_2,\ldots,m_N}) \in \mathbb{R}^{O \times I}$$

where $\boldsymbol{p}_{m_1,m_2,\ldots,m_N} = (g_{1,m_1}\ g_{2,m_2}\ \cdots\ g_{N,m_N})$. Superscript s means "sampled." Store the sampled matrices $\boldsymbol{S}^s_{m_1,m_2,\ldots,m_N}$ into the tensor $\mathcal{S}^s \in \mathbb{R}^{M_1 \times M_2 \times \cdots \times M_N \times O \times I}$.

Step 2. Extracting the LTI vertex systems. This step uses higher-order singular value decomposition (HOSVD) extended with transformations NN (nonnegativeness), SN (sum normalization), and NO (normality). The studies of HOSVD can be found in a large varieties of publications. This paper uses the concept and tensor notation of HOSVD as discussed in Ref. 1. The SN, NN, and NO transformations are introduced in Refs. 27 and 28.

This step executes the extended HOSVD on the first N dimensions of tensor $\mathcal{S}^s$. While performing the HOSVD we discard all zero or small singular values σ_k and their corresponding singular vectors in all dimensions. As a result we have

$$\mathcal{S}^s \underset{\gamma}{\approx} \mathcal{S} \underset{n}{\otimes} \boldsymbol{U}_n$$

where the error γ is bounded as

$$\gamma = \left(\left\|\mathcal{S}^s - \mathcal{S} \underset{n}{\otimes} \boldsymbol{U}_n\right\|_{L_2}\right)^2 \le \sum_k \sigma_k^2 \tag{14}$$

The resulting tensor $\mathcal{S}$, with the size of $(I_1 \times I_2 \times \cdots \times I_N \times O \times I)$, where $\forall n : I_n \le M_n$, contains the LTI vertex systems, and is immediately substitutable into relation (8). The NN and SN transformations guarantee that the resulting LTI vertex systems form a convex hull of the sampled systems in $\mathcal{S}^s$. When the transformation NO is executed, the resulting LTI systems form the tight convex hull of the sampled systems.

The software implementations of HOSVD, NN, SN, and NO are rather simple, for instance, in MATLAB programing.

Step 3. Constructing continuous basis system. One can determine the discretized points of the basis easily from matrices $\boldsymbol{U}_n$. The i_nth column vector $\boldsymbol{u}_{n,i_n=1\ldots I_n}$ of matrix $\boldsymbol{U}_n \in \mathbb{R}^{M_n \times I_n}$ determines one discretized basis function $w_{n,i_n}[p_n(t)]$ of variable $p_n(t)$. The values u_{n,m_n,i_n} of column i_n define the values of the basis function $w_{n,i_n}(p_n(t))$ over the gridlines $p_n(t) = g_{n,m_n}$:

$$w_{n,i_n}\left(g_{n,m_n}\right) = u_{n,m_n,i_n}$$

The basis functions can be determined over any points by the help of the given $\boldsymbol{S}(\boldsymbol{p}(t))$. To determine the basis functions in vector $\boldsymbol{w}_d(p_d)$, let p_k be fixed to the gridlines as

$$p_k = g_{k,1}, \qquad k = 1 \ldots N, \qquad k \ne d$$

Then for p_d,

$$\boldsymbol{w}_d(p_d) = [\boldsymbol{S}(\boldsymbol{p})]_{(1)} \left[\left(\mathcal{S} \underset{k}{\otimes} \boldsymbol{u}_{k,1}\right)_{(n)}\right]^+$$

where vector $\boldsymbol{p}$ consists of elements p_k and p_d as $\boldsymbol{p} = (g_{1,1}\ g_{2,1}\ \cdots\ p_d\ \cdots\ g_{N,1})$, the superscript $+$ denotes pseudo inverse, and $\boldsymbol{u}_{k,1}$ is the first row vector of $\boldsymbol{U}_k$. The first mode matrix $(\boldsymbol{S}(\boldsymbol{p}))_{(1)}$ of matrix $\boldsymbol{S}(\boldsymbol{p})$ is understood such that matrix $\boldsymbol{S}(\boldsymbol{p}) \in \mathbb{R}^{O \times I}$ is considered as a three-dimensional tensor $\mathcal{S}(\boldsymbol{p}) \in \mathbb{R}^{1 \times O \times I}$, where the length of the first dimension is 1. $\boldsymbol{S}(\boldsymbol{p})_{(1)}$ practically means that the matrix $\boldsymbol{S}(\boldsymbol{p})$ is stored into one row vector by placing the rows of $\boldsymbol{S}(\boldsymbol{p})$ next to each other.

TP Model of the Prototypical Aeroelastic Wing Section

We execute method 1 on model (4). First, according to method 1, let us define the transformation space Ω. We are interested in the interval $U \in [14, 25]$ m/s and we presume that the interval $\alpha \in [-0.1, 0.1]$ rad is sufficiently large. This has practical significance because the prototypical aeroelastic model (4) is accurate for low speeds. Therefore, let $\Omega : [14, 25] \times [-0.1, 0.1]$ in the present example (note that these intervals can be arbitrarily extended). Let the grid density be defined as $M_1 \times M_2$, $M_1 = 100$, and $M_2 = 100$. By executing step 2 of method 1, one can see that the rank of the sampled tensor $\mathcal{S}^s \in \mathbb{R}^{M_1 \times M_2 \times 4 \times 4}$ on the first dimension is 3 and on the second dimension is 2. The nonzero-singular values of the first dimension are 16,808, 1442, 2. The nonzero-singular values of the second dimension are 13,040, 7970. By discarding only zero-singular values (we discard 97 zero-singular values on the first and 98 zero-singular values on the second dimension, and we keep all the nonzero-singular values), the sizes of the resulting matrices $\boldsymbol{U}_1$ and $\boldsymbol{U}_2$ are $(M_1 \times 3)$ and $(M_2 \times 2)$, respectively. The basis functions

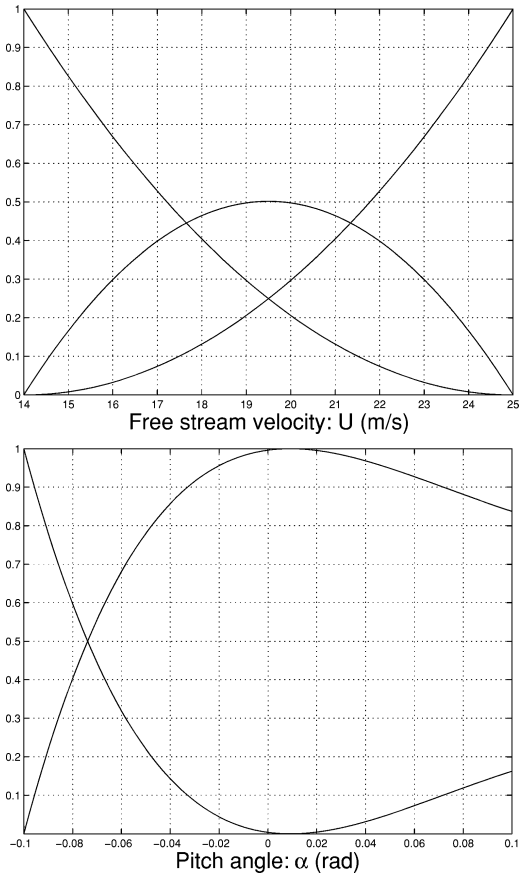

Fig. 3 Basis functions of the dimensions U and α.

$w_{1,i}(U)$, $i = 1 \ldots 3$, and $w_{2,j}(\alpha)$, $j = 1 \ldots 2$, computed by the third step of the TP-model transformation are depicted in Fig. 3. The $3 \times 2 = 6$ LTI systems are

$$\boldsymbol{A}_{1,1} = 10^3 \begin{pmatrix} 0 & 0 & 0.0010 & 0 \\ 0 & 0 & 0 & 0.0010 \\ -0.2314 & -0.0095 & -0.0034 & -0.0001 \\ 0.2780 & -1.1036 & 0.0071 & -0.0000 \end{pmatrix}$$

$$\boldsymbol{B}_{1,1} = \begin{pmatrix} 0 \\ 0 \\ -8.5825 \\ -32.4370 \end{pmatrix}$$

$$\boldsymbol{A}_{2,1} = \begin{pmatrix} 0 & 0 & 1.0000 & 0 \\ 0 & 0 & 0 & 1.0000 \\ -231.3804 & -46.3063 & -4.3776 & -0.2573 \\ 277.9906 & -966.7931 & 10.6520 & 0.4104 \end{pmatrix}$$

$$\boldsymbol{B}_{2,1} = \begin{pmatrix} 0 \\ 0 \\ -27.3677 \\ -103.4344 \end{pmatrix}$$

$$\boldsymbol{A}_{3,1} = 10^3 \begin{pmatrix} 0 & 0 & 0.0010 & 0 \\ 0 & 0 & 0 & 0.0010 \\ -0.2314 & -0.0227 & -0.0039 & -0.0002 \\ 0.2780 & -1.0543 & 0.0089 & 0.0002 \end{pmatrix}$$

$$\boldsymbol{B}_{3,1} = 10^3 \begin{pmatrix} 0 \\ 0 \\ -0.0154 \\ -0.0580 \end{pmatrix}$$

$$\boldsymbol{A}_{1,2} = \begin{pmatrix} 0 & 0 & 1.0000 & 0 \\ 0 & 0 & 0 & 1.0000 \\ -231.3804 & -16.5786 & -3.4333 & -0.1425 \\ 277.9906 & 23.0842 & 7.1447 & -0.0157 \end{pmatrix}$$

$$\boldsymbol{B}_{1,2} = \begin{pmatrix} 0 \\ 0 \\ -8.5825 \\ -32.4370 \end{pmatrix}$$

$$\boldsymbol{A}_{2,2} = \begin{pmatrix} 0 & 0 & 1.0000 & 0 \\ 0 & 0 & 0 & 1.0000 \\ -231.3804 & -53.4094 & -4.3776 & -0.2573 \\ 277.9906 & 159.8695 & 10.6520 & 0.4104 \end{pmatrix}$$

$$\boldsymbol{B}_{2,2} = \begin{pmatrix} 0 \\ 0 \\ -27.3677 \\ -103.4344 \end{pmatrix}$$

$$\boldsymbol{A}_{3,2} = \begin{pmatrix} 0 & 0 & 1.0000 & 0 \\ 0 & 0 & 0 & 1.0000 \\ -231.3804 & -29.8524 & -3.9054 & -0.1999 \\ 277.9906 & 72.3823 & 8.8983 & 0.1974 \end{pmatrix}$$

$$\boldsymbol{B}_{3,2} = \begin{pmatrix} 0 \\ 0 \\ -15.3526 \\ -58.0244 \end{pmatrix}$$

Note that the rank of the first two dimensions of the sampled tensor $\mathcal{S}^s$ are always three and two, respectively, independent of how we increase the density of the sampling grid. When we numerically check the error between the model (4) and the resulting TP model, we find that the error is about 10^{-11} of that which is caused by the numerical computation. One can see that the third singular value of the first dimension is relatively very small. One may decrease the dimensionality by discarding it. This yields 2×2 basis system. In this case the resulting model is not exact.

In conclusion, the aeroelastic model (4) can be described exactly in finite convex TP form of six vertex LTI models. Note that one may try to derive the basis functions analytically from relation (3). The basis functions of α can be extracted from $k_\alpha(\alpha)$. Finding the basis functions of U, however, is rather complicated. Finding the tight convex hull via analytic derivations may also be very hard work. In spite of this, the computation of the TP model transformation takes a few seconds. It should be emphasized that the TP model transformation does not depend on the analytic model. It could be executed on more complex physical or black-box aeroelastic model, and the resulting TP model may contain different and probably more LTI systems than the present example, or may not result in an exact TP model but in a TP model with an acceptable accuracy if enough number singular values are kept.

Determination of Controllers via Parallel Distributed Compensation

In the previous section we transformed the aeroelastic model (4) to TP-model form whereupon LMI design under the PDC framework can be executed immediately. This section briefly introduces the main concept of the LMI design and calls LMI design theorems involving different control purposes.

As a result of the dramatic and continuing growth in computer power and the advent of very powerful algorithms (and associated theory) for convex optimization, we can now solve very rapidly many convex optimization problems involving LMIs.[29] Many control problems and design specifications have LMI formulations[30,31] that come from the fact that LMI formulations have the ability

to readily combine various design constraints or objectives in a numerical tractable manner. This is especially true for Lyapunov-based analysis and design, but also for optimal LQG control,[30] robust H_2/H_∞ control,[32,33] multimodel/multiobjective state feedback design,[30,34–37] covariance control, robust gain-scheduled control, control of stochastic systems.[30] A great list of related publications and problems, which can be solved via LMIs, is addressed in Ref. 23. Some authors[30] claim that once a control problem is formulated in terms of LMIs then the problem is solved and point out that the LMI-based controller design leads to solutions even in cases where analytic solutions do not exist. (Multiple Riccati equations cannot be solved analytically in general.) Further developments of LMIs for these design problems are an area of active research. Commercialized software for LMI-based design are available for engineering practices.[23]

As an alternative way of LMI-based robust-control design, the PDC framework was introduced by Tanaka and Wang.[22] The PDC design framework determines one LTI feedback gain to each LTI vertex system of a given convex TP model. The framework starts with the LTI vertex systems $\mathcal{S}$ and results in the vertex LTI gains $\mathcal{K}$ of the controller. The $\mathcal{K}$ is computed by the LMI-based stability theorems. The PDC framework determines the control value by the same basis functions as used in relation (8) and by $\mathcal{K}$ such as

$$\boldsymbol{u}(t) = -\left\{\mathcal{K} \overset{N}{\underset{n=1}{\otimes}} \boldsymbol{w}_n[p_n(t)]\right\}\boldsymbol{x}(t) \tag{15}$$

The LMI theorems, to be solved under the PDC framework, are selected according to the stability criteria and the desired control performance. For instance, the speed of response and constraints on the state vector or on the control value can be considered via properly selected LMI-based stability theorems. The present control design applies different LMI theorems to achieve asymptotic stability and to enforce constraints on the control value for the present aeroelastic system.

Let us recall briefly those LMI theorems that will be applied here. The derivations and the proofs of these theorems are fully detailed in Ref. 21. Before dealing with the LMI theorems, we introduce a simple indexing technique to have a direct link between the TP-model form and the typical form of LMI formulations:

Method 2: Index transformation.

Let

$$\boldsymbol{S}_r = \begin{pmatrix} \boldsymbol{A}_r & \boldsymbol{B}_r \\ \boldsymbol{C}_r & \boldsymbol{D}_r \end{pmatrix} = \boldsymbol{S}_{i_1,i_2,\ldots,i_N}$$

where $r = \text{ordering}\,(i_1, i_2, \ldots, i_N)\,(r = 1 \ldots R = \prod_n I_n)$. The function "ordering" results in the linear index equivalent of an N-dimensional array's index $i_1, i_2, \ldots, i_N$, when the size of the array is $I_1 \times I_2 \times \cdots \times I_N$. Let the basis functions be defined according to the sequence of r:

$$w_r[\boldsymbol{p}(t)] = \prod_n w_{n,i_n}[p_n(t)]$$

First we call one of the simplest LMI design theorems. The controller design can be derived from the Lyapunov stability theorems for global and asymptotic stability as shown in Ref. 22:

Theorem 1: Global and asymptotic stabilization of the convex TP model (8). Assume a given state-space model in TP form (8) with conditions (11) and (12).

Find $\boldsymbol{X} > 0$ and $\boldsymbol{M}_r$ satisfying

$$-\boldsymbol{X}\boldsymbol{A}_r^T - \boldsymbol{A}_r\boldsymbol{X} + \boldsymbol{M}_r^T\boldsymbol{B}_r^T + \boldsymbol{B}_r\boldsymbol{M}_r > 0 \tag{16}$$

for all r and

$$-\boldsymbol{X}\boldsymbol{A}_r^T - \boldsymbol{A}_r\boldsymbol{X} - \boldsymbol{X}\boldsymbol{A}_s^T - \boldsymbol{A}_s\boldsymbol{X} + \boldsymbol{M}_s^T\boldsymbol{B}_r^T + \boldsymbol{B}_r\boldsymbol{M}_s + \boldsymbol{M}_r^T\boldsymbol{B}_s^T + \boldsymbol{B}_s\boldsymbol{M}_r \geq 0 \tag{17}$$

for $r < s \leq R$, except the pairs (r, s) such that $w_r[\boldsymbol{p}(t)]w_s[\boldsymbol{p}(t)] = 0, \forall \boldsymbol{p}(t)$.

Because the above conditions (16) and (17) are LMIs with respect to variables $\boldsymbol{X}$ and $\boldsymbol{M}_r$, we can find a positive definite matrix $\boldsymbol{X}$ and matrix $\boldsymbol{M}_r$ or determine that no such matrices exist. This is a convex feasibility problem. Numerically, this problem can be solved very efficiently by means of the most powerful tools available in the mathematical programming literature such as MATLAB LMI toolbox.[23] The feedback gains can be obtained from the solutions $\boldsymbol{X}$ and $\boldsymbol{M}_r$ as

$$\boldsymbol{K}_r = \boldsymbol{M}_r\boldsymbol{X}^{-1} \tag{18}$$

Then, by the help of $r = \text{ordering}\,(i_1, i_2, \ldots, i_N)$ in method 2, one can define feedbacks $\boldsymbol{K}_{i_1,i_2,\ldots,i_N}$ from $\boldsymbol{K}_r$ obtained in relation (18) and store into tensor $\mathcal{K}$ of relation (15).

The speed of response is related to decay rate; that is the largest Lyapunov exponent. The largest lower bound on the decay rate that we can find using a quadratic Lyapunov function can be found by solving the following generalized eigenvalue minimization problem.

Theorem 2: Decay rate optimization.

$$\underset{X, M_1, \ldots, M_1}{\text{maximize}}\ \alpha \quad \text{subject to}$$

$$-\boldsymbol{X}\boldsymbol{A}_r^T - \boldsymbol{A}_r\boldsymbol{X} + \boldsymbol{M}_r^T\boldsymbol{B}_r^T + \boldsymbol{B}_r\boldsymbol{M}_r - 2\alpha\boldsymbol{X} > 0 \tag{19}$$

for all r and

$$-\boldsymbol{X}\boldsymbol{A}_r^T - \boldsymbol{A}_r\boldsymbol{X} - \boldsymbol{X}\boldsymbol{A}_s^T - \boldsymbol{A}_s\boldsymbol{X} + \boldsymbol{M}_s^T\boldsymbol{B}_r^T + \boldsymbol{B}_r\boldsymbol{M}_s + \boldsymbol{M}_r^T\boldsymbol{B}_s^T + \boldsymbol{B}_s\boldsymbol{M}_r - 4\alpha\boldsymbol{X} \geq 0 \tag{20}$$

for $r < s \leq R$, except the pairs (r, s) such that $w_r[\boldsymbol{p}(t)]w_s[\boldsymbol{p}(t)] = 0, \forall \boldsymbol{p}(t)$. The feedback gains can be obtained form the solutions $\boldsymbol{X}$ and $\boldsymbol{M}_r$; see relation (18).

To set constrains on the control value we add the following LMIs to relations (16) and (17) or relations (19) and (20):

Theorem 3: Constraint on the control value. Assume that $\|\boldsymbol{x}(0)\| \leq \phi$, where $\boldsymbol{x}(0)$ is unknown but the upper bound ϕ is known. The constrain $\|\boldsymbol{u}(t)\| \leq \mu$ is enforced at all times $t > 0$ if the LMIs

$$\phi^2\boldsymbol{I} \leq \boldsymbol{X}, \qquad \begin{pmatrix} \boldsymbol{X} & \boldsymbol{M}_i^T \\ \boldsymbol{M}_i & \mu^2\boldsymbol{I} \end{pmatrix} \geq 0$$

hold. We obtain the feedback gains as in relation (18) by solving all the LMIs.

Evaluation of the Derived Controllers

To demonstrate the performance of the controlled system, numerical experiments are presented in this subsection. To be comparable to other published results and figures of the control results, the numerical examples are performed with $a = -0.4$ and with free stream velocity and $U = 20$ m/s, a velocity which exceeds the linear flutter velocity $U = 15.5$ m/s, and for initials $h = 0.01$ m and $\alpha = 0.1$ rad. The control values β (rad) are computed by model (15) as

$$u(t) = -\left(\sum_{i=1}^{3}\sum_{j=1}^{2} w_{1,i}[U(t)]w_{2,j}[\alpha(t)]\boldsymbol{K}_{i,j}\right)\boldsymbol{x}(t) \tag{21}$$

in all cases of the simulations. Vectors $\boldsymbol{K}_{i,j}$ result from LMIs discussed in the preceding section.

Controller 1: Global and asymptotic stabilization of the aeroelastic model. Let the resulting LTI vertex systems be substituted into the LMIs of theorem 1. The LMI solvers shows that Eqs. (16) and (17) are feasible in the present case:

$$\boldsymbol{X} = 10^8 \begin{pmatrix} 0.0213 & 0.0023 & -0.0217 & -0.0506 \\ 0.0023 & 0.0172 & 0.0278 & -0.1131 \\ -0.0217 & 0.0278 & 6.0189 & -0.8293 \\ -0.0506 & -0.1131 & -0.8293 & 4.2114 \end{pmatrix}$$

Equation (18) yields six LTI feedback gains $\boldsymbol{K}_{i,j}$:

$$\boldsymbol{K}_{1,1} = (-6.9079 \quad 9.8289 \quad -0.1545 \quad -1.1896)$$

$$\boldsymbol{K}_{2,1} = (-2.1000 \quad 5.7063 \quad -0.1551 \quad -0.1848)$$

$$\boldsymbol{K}_{3,1} = (-3.8807 \quad 11.2178 \quad -0.1065 \quad -0.2071)$$

$$\boldsymbol{K}_{1,2} = (-5.9511 \quad -5.1286 \quad -0.1845 \quad -0.6240)$$

$$\boldsymbol{K}_{2,2} = (-2.6178 \quad -8.2716 \quad -0.3337 \quad -0.4773)$$

$$\boldsymbol{K}_{3,2} = (-4.0982 \quad -4.1592 \quad -0.1081 \quad -0.3394)$$

Figure 4 shows the time response of the controlled system. One can observe the asymptotic stabilization and $\alpha(t)$ that smoothly converges to zero. An important issue should be addressed here. Theorem 1 claims that the resulting controller is globally stable. However, the TP-model transformation is a numerical method that can be performed over an arbitrary, but bounded, domain Ω. Therefore, the global stability, ensured by theorem 1, is restricted to Ω and, hence, becomes local stability. This, however, has practical significance because the accuracy of a given model is also bounded in reality. In the present example the prototypical aeroelastic model is accurate only for low speeds, and we have defined Ω accordingly in the design process. The resulting controller guarantees asymptotic

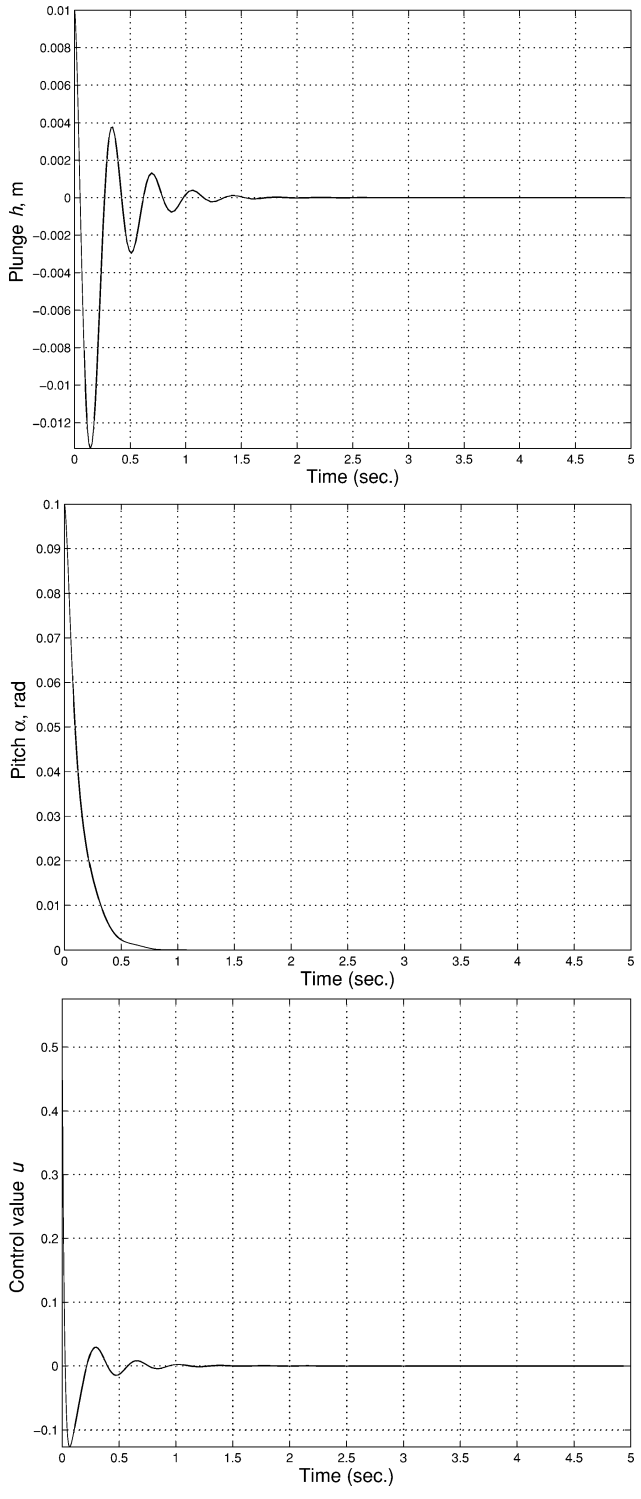

Fig. 4 Time response of controller 1 for $U = 20$ m/s and $a = -0.4$.

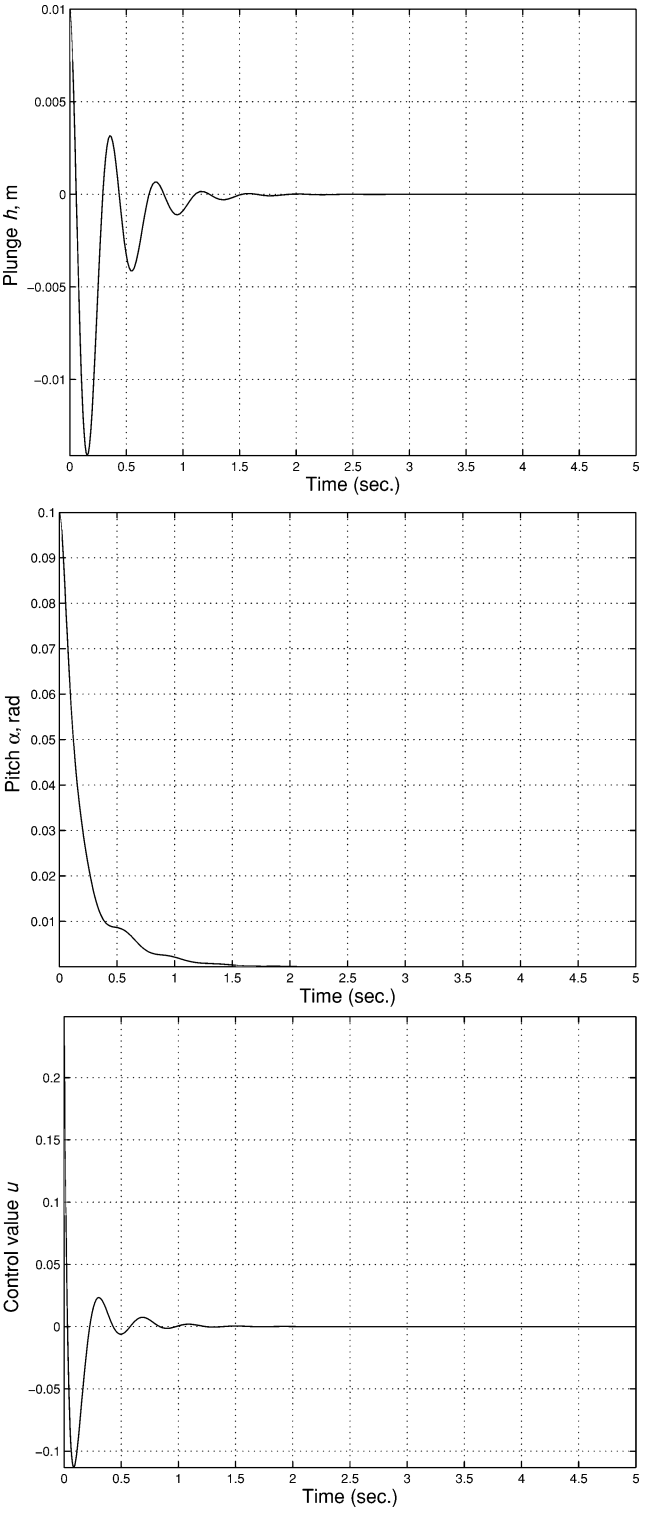

Fig. 5 Time response of controller 2 "min" for $U = 20$ m/s and $a = -0.4$.

stability in $\Omega : [14; 25] \times [-0.1, 0.1]$. One may extend Ω and execute the design method again.

Controller 1.1: Decay rate control. When we apply theorem 2 we find that $\alpha = 0$ in the present case. This simply means that the LMIs in theorem 2 become equivalent to the LMIs of theorem 1. The resulting controller will also be equivalent to the controller 1.

Controller 2: Constraint on the control value. To bound the control values we apply theorem 3. In the case of controller 2 "min" we searched the minimal bound of the control value while the LMIs are feasible. The response of the resulting controller is presented on Fig. 5. The maximum control value is 0.25. This is significantly smaller than in the case of controller 1. Obviously, we can see that the stabilization time is more than twice as long.

For comparison we derive controller 2 "max," where we apply a tenfold larger bound. The response of the resulting controller is presented on the Fig. 6. The maximum control value is 2.15. One can observe that the stabilization time becomes considerable smaller than on the previous figures.

We select the control result of the exact feedback linearization technique for comparison; see Secs. IV.A and IV.B of Ref. 12. The reason we selected this technique is that it applies a single control surface like the present method. Figure 7 presents the time response

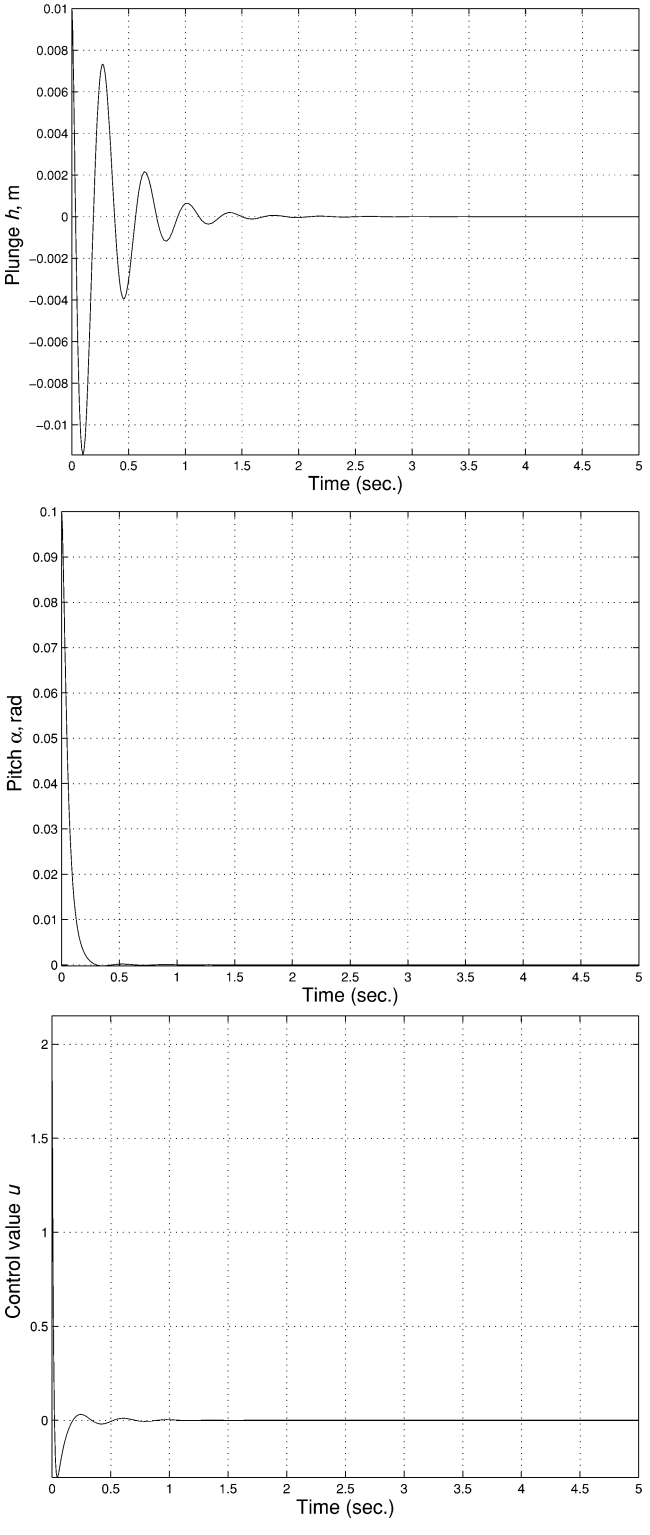

Fig. 6 Time response of controller 2 "max" for $U = 20$ m/s and $a = -0.4$.

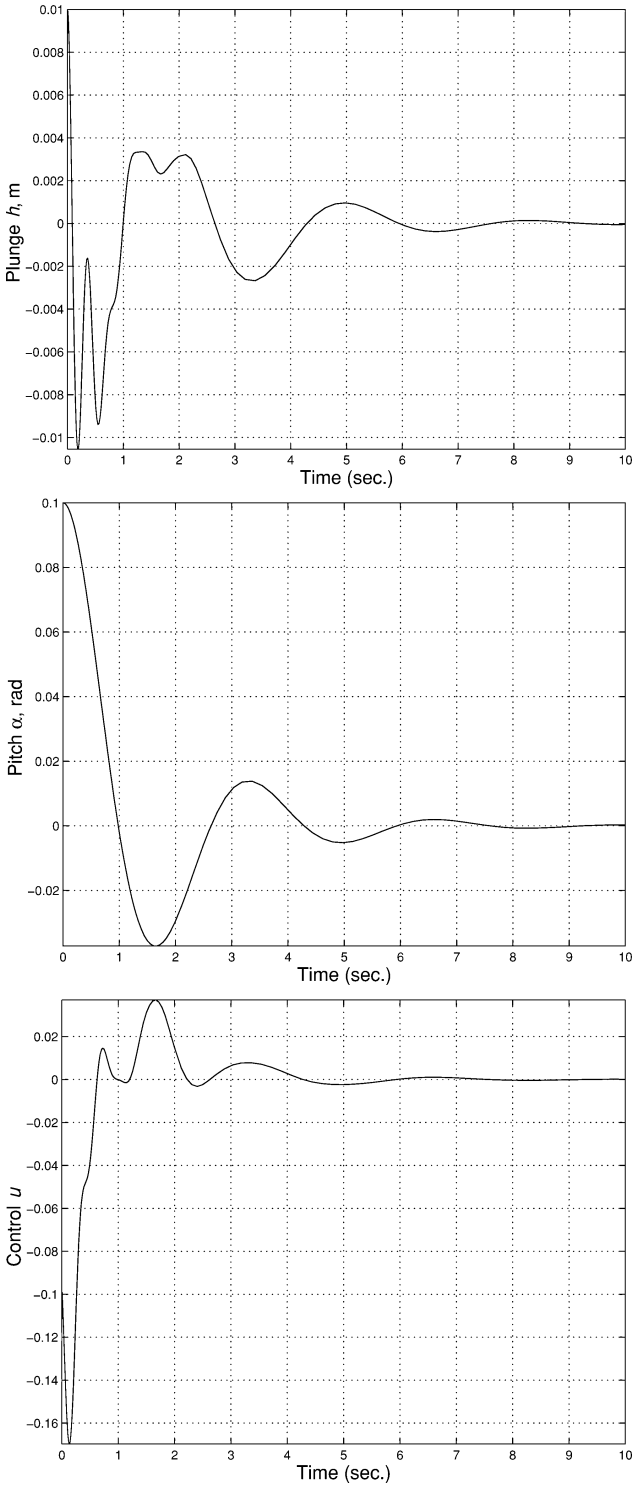

Fig. 7 Time response by the exact feedback linearization method for $U = 20$ m/s and $a = -0.4$.

of the controller, developed via exact feedback linearization. By comparing the control results, one can observe that the controllers developed in this paper are considerable faster. One can also observe that α converges smoothly to zero on Figs. 4–6, as opposed to the values of α on Fig. 7. Note that we applied very simple LMI theorems. To achieve more advantageous control results, various further performance specifications can be ensured by selecting more powerful LMI design theorems.[22] Former solutions of this aeroelastic control problem do not offer the chance to consider further control specifications beyond stability.

Conclusions

This paper investigates the advantages of a recently proposed numerical control design method in the case of the prototypical aeroelastic wing section. To show these advantages, we derive controllers for different control specifications and show that the present control design is executable in a few minutes, is capable of involving various control specifications beyond stability, and results in an exact alternative tensor-product model description, which opens a gate to various recent linear-matrix-inequality-based design frameworks. According to the nature of the control design method, it is irrelevant whether the given explicit model is a physical model or just an outcome of black-box (for instance, neural net) identification. Thus, the general conclusions drawn from the present design steps could be promising in different and more complex aeroelastic systems as well.

Appendix: System Parameters and Variables of the Aeroelastic Model

System Parameters

$$b = 0.135\,\text{m}, \qquad \text{span} = 0.6\,\text{m}, \qquad k_h = 2844.4\,\text{N/m}$$

$$c_h = 27.43\,\text{Ns/m}, \qquad c_\alpha = 0.036\,\text{Ns}, \qquad \rho = 1.225\,\text{kg/m}^3$$

$$c_{l_\alpha} = 6.28, \qquad c_{l_\beta} = 3.358, \qquad c_{m_\alpha} = (0.5 + a)c_{l_\alpha}$$

$$c_{m_\beta} = -0.635, \qquad m = 12.387\,\text{kg}, \qquad x_\alpha = -0.3533 - a$$

$$I_\alpha = 0.065\,\text{kgm}^2, \qquad c_\alpha = 0.036$$

System Variables

$$d = m\left(I_\alpha - m x_\alpha^2 b^2\right), \qquad k_1 = I_\alpha k_h / d$$

$$k_2 = \left(I_\alpha \rho b c_{l_\alpha} + m x_\alpha b^3 \rho c_{m_\alpha}\right)/d, \qquad k_3 = -m x_\alpha b k_h / d$$

$$k_4 = \left(-m x_\alpha b^2 \rho c_{l_\alpha} - m \rho b^2 c_{m_\alpha}\right)/d, \qquad p(\alpha) = (-m x_\alpha b/d) k_\alpha(\alpha)$$

$$q(\alpha) = (m/d) k_\alpha(\alpha)$$

$$c_1(U) = \left[I_\alpha\left(c_h + \rho U b c_{l_\alpha}\right) + m x_\alpha \rho U^3 c_{m_\alpha}\right]/d$$

$$c_2(U) = \left(I_\alpha \rho U b^2 c_{l_\alpha}\left(\tfrac{1}{2} - a\right) - m x_\alpha b c_\alpha + m x_\alpha \rho U b^4 c_{m_\alpha}\left(\tfrac{1}{2} - a\right)\right)/d$$

$$c_3(U) = \left(-m x_\alpha b c_h - m x_\alpha \rho U b^2 c_{l_\alpha} - m \rho U b^2 c_{m_\alpha}\right)/d$$

$$c_4(U) = \left(m c_\alpha - m x_\alpha \rho U b^3 c_{l_\alpha}\left(\tfrac{1}{2} - a\right) - m \rho U b^3 c_{m_\alpha}\left(\tfrac{1}{2} - a\right)\right)/d$$

$$g_3 = \left(-I_\alpha \rho b c_{l_\beta} - m x_\alpha b^3 \rho c_{m_\beta}\right)/d$$

$$g_4 = \left(m x_\alpha b^2 \rho c_{l_\beta} + m \rho b^2 c_{m_\beta}\right)/d$$

Acknowledgments

This research was supported by Hungarian Scientific Research Fund (OTKA) F 49838.

References

[1]Lathauwer, L. D., Moor, B. D., and Vandewalle, J., "A Multi Linear Singular Value Decomposition," *Journal on Matrix Analysis and Applications*, Vol. 21, No. 4, 2000, pp. 1253–1278.

[2]Price, S. J., Alighanbari, H., and Lee, B. H. K., "Postinstability Behavior of a Two-Dimensional Airfoil with a Structural Nonlinearity of Aircraft," *Journal of Aircraft*, Vol. 31, No. 6, 1994, pp. 1395–1401.

[3]Price, S. J., Alighanbari, H., and Lee, B. H. K., "The Aeroelastic Response of a Two-Dimensional Airfoil with Bilinear and Cubic Structural Nonlinearities," *Proceedings of the 35th AIAA Structures, Structural Dynamics, and Matirials Conference*, AIAA, Washington, DC, 1994, pp. 1771–1780.

[4]Lee, B. H. K., and LeBlanc, P., "Flutter Analysis of a Two-Dimensional Airfoil: The Cubic Non-Linear Restoring Force," National Aeronautical Estalishment, Aeronautical Note-36, NRC No. 25336, National Research Council, Ottawa, 1986.

[5]Zhao, L. C., and Yang, Z. C., "Chaotic Motions of an Airfoil with Nonlinear Stiffness in Incompressible Flow," *Journal of Sound and Vibration*, Vol. 138, No. 2, 1990, pp. 245–254.

[6]O'Neil, T., and Strganac, T. W., "An Experimental Investigation of Nonlinear Aeroelastic Response," *Proceedings of the 36th AIAA/ASME/ASCE/AHS/ASC Structures, Structural Dynamics, and Materials Conference*, AIAA, Washington, DC, 1995, pp. 2043–2051.

[7]Marzocca, P., and Librescu, L., "Aeroelastic Response of Nonlinear Wing Sections Using a Functional Series Technique," *AIAA Journal*, Vol. 40, No. 5, 2002, pp. 813–824.

[8]Block, J. J., and Strganac, T. W., "Applied Active Control for Nonlinear Aeroelastic Structure," *Journal of Guidance, Control, and Dynamics*, Vol. 21, No. 6, 1998, pp. 838–845.

[9]Waszak, M. R., "Robust Multivariable Flutter Suppression for the Benchmark Active Control Technology (BACT) Wind-Tunnel Model," *Journal of Guidance, Control, and Dynamics*, Vol. 24, No. 1, 1997, pp. 147–143.

[10]Mukhopadhyay, V., "Transonic Flutter Suppression Control Law Design and Wind-Tunnel Test Results," *Journal of Guidance, Control, and Dynamics*, Vol. 23, No. 5, 2000, pp. 930–937.

[11]Kelkar, A. G., and Joshi, S. M., "Passivity-Based Robust Control with Application to Benchmark Controls Technology Wing," *Journal of Guidance, Control, and Dynamics*, Vol. 23, No. 5, 2000, pp. 938–947.

[12]Ko, J., Kurdila, A. J., and Strganac, T. W., "Nonlinear Control of a Prototypical Wing Section with Torsional Nonlinearity," *Journal of Guidance, Control, and Dynamics*, Vol. 20, No. 6, 1997, pp. 1181–1189.

[13]Ko, J., Kurdila, A. J., and Strganac, T. W., "Adaptive Feedback Linearization for the Control of a Typical Wing Section with Structural Nonlinearity," *Journal of Guidance, Control, and Dynamics*, Vol. 21, No. 5, 1998, pp. 718–725.

[14]Xing, W., and Singh, S. N., "Adaptive Output Feedback Control of a Nonlinear Aeroelastic Structure," *Journal of Guidance, Control, and Dynamics*, Vol. 23, No. 6, 2000, pp. 1109–1116.

[15]Ko, J., Kurdila, A. J., and Strganac, T. W., "Nonlinear Control Theory for a Class of Structural Nonlinearities in a Prototypical Wing Section," AIAA Paper 97-0580, Jan. 1997.

[16]O'Neil, T., Gilliat, H. C., and Strganac, T. W., "Investigations of Aeroelastic Response for a System with Continuous Structural Nonlinearities," AIAA Paper 96-1390, April 1996.

[17]Ko, J., and Strganac, T. W., "Stability and Control of a Structurally Nonlinear Aeroelastic System," *Journal of Guidance, Control, and Dynamics*, Vol. 21, No. 5, 1998, pp. 718–725.

[18]Yim, W., Singh, S. N., and Wells, W., "Nonlinear Control of a Prototypical Aeroelastic Wing Section: State-Dependent Riccati Equation Method," *International Conference on Nonlinear Problems in Aviation and Aerospace (ICNPAA'02)*, May 2002, pp. 543–550.

[19]Scott, R. C., and Pado, L. E., "Active Control of Wind-Tunnel Model Aeroelastic Response Using Neural Networks," *Journal of Guidance, Control, and Dynamics*, Vol. 23, No. 6, 2000, pp. 1100–1108.

[20]Baranyi, P., Tikk, D., Yam, Y., and Patton, R. J., "From Differential Equations To PDC Controller Design via Numerical Transformation," *Computers in Industry*, Vol. 51, 2003, pp. 281–297.

[21]Baranyi, P., "TP Model Transformation as a Way To LMI-Based Controller Design," *IEEE Transactions on Industrial Electronics*, Vol. 51, No. 2, 2004, pp. 387–400.

[22]Tanaka, K., and Wang, H. O., *Fuzzy Control Systems Design and Analysis—A Linear Matrix Inequality Approach*, Wiley, New York, 2001.

[23]Gahinet, P., Nemirovski, A., Laub, A. J., and Chilali, M., *LMI Control Toolbox*, MathWorks, Natick, MA, 1995.

[24]Fung, Y. C., *An Introduction To the Theory of Aeroelasticity*, Wiley, New York, 1955.

[25]Dowell, E. H., Curtiss, H. C. J., Scanlan, R. H., and Sisto, F. (eds.), *A Modern Course in Aeroelasticity*, Stifthoff and Noordhoff, Alpen aan den Rijn, The Netherlands, 1978.

[26]Tikk, D., Baranyi, P., Patton, R. J., and Tar, J., "Approximation Capability of TP Model Forms," *Australian Journal of Intelligent Information Processing Systems*, Vol. 8, No. 3, 2004, pp. 155–163.

[27]Yam, Y., Baranyi, P., and Yang, C. T., "Reduction of Fuzzy Rule Base via Singular Value Decomposition," *IEEE Transactions on Fuzzy Systems*, Vol. 7, No. 2, 1999, pp. 120–132.

[28]Yam, Y., Yang, C. T., and Baranyi, P., "Singular Value-Based Fuzzy Reduction with Relaxed Normalization Condition," *Interpretability Issues in Fuzzy Modeling*, J. Casillas, O. Cordn, F. Herrera, and L. Magdalena (eds.), Vol. 128, Studies in Fuzziness and Soft Computing, Springer-Verlag, 2003, pp. 325–354.

[29]Nesterov, Y., and Nemirovsky, A., *Interior-Point Polynomial Methods in Convex Programing: Theory and Applications*, SIAM Books, Philadelphia, 1994.

[30]Boyd, S., Ghaoui, L. E., Feron, E., and Balakrishnan, V., "Linear Matrix Inequalities in System and Control Theory," Society for Industrial and Applied Mathematics, Philadelphia, 1994.

[31]Ghaoui, L. E., and Niculescu, S. I., *Advances in Linear Matrix Inequality Methods in Control*, Advances in Design and Control, Society for Industrial and Applied Mathematics, Philadelphia, 2000.

[32]Gahinet, P., and Apkarian, P., "A Linear Matrix Inequality Approach To H_∞ Control," *International Journal on Robust and Nonlinear Control*, Vol. 4, 1994, pp. 421–448.

[33]Iwasaki, T., and Skelton, R., "All Controllers for the General H_∞ Control Problem: LMI Existence Conditions and State-Space Formulas," *Automatica*, Vol. 30, No. 8, 1994, pp. 1307–1317.

[34]Barmish, B., "Stabilization of Uncertain Systems via Linear Control," *IEEE Transactions on Automation and Control*, Vol. AC-28, Aug. 1983, pp. 848–850.

[35]Chilali, M., and Gahinet, P., "H_∞ Design with Pole Placement Constrains: An LMI Approach," *IEEE Transactions on Automation and Control*, Vol. 41, No. 3, 1996, pp. 358–367.

[36]Khargonekar, P., and Rotea, M., "Mixed H_2/H_∞," *IEEE Transactions on Automation and Control*, Vol. 39, 1991, pp. 824–837.

[37]Scherer, C. W., Gahinet, P., and Chilali, M., "Multi-Objective Output-Feedback Control via LMI Optimization," *IEEE Transactions on Automation and Control*, Vol. 42, 1997, pp. 896–911.